Journal of Solid State Chemistry 181 (2008) 3264–3268

Contents lists available at ScienceDirect

Journal of Solid State Chemistry

journal homepage: www.elsevier.com/locate/jssc

Synthesis of nanocrystalline $REBO_3$ (RE = Y, Nd, Sm, Eu, Gd, Ho) and YBO_3:Eu using a borohydride-based solution precursor route

Amanda E. Henkes [a], Raymond E. Schaak [a,b,*]

[a] Department of Chemistry, Texas A&M University, College Station, TX 77842-3012, USA
[b] Department of Chemistry, The Pennsylvania State University, University Park, PA 16802, USA

ARTICLE INFO

Article history:
Received 7 May 2008
Received in revised form
12 August 2008
Accepted 17 August 2008
Available online 2 September 2008

Keywords:
Rare-earth borates
Solution precursors
Low temperature synthesis
Phosphors

ABSTRACT

A solution precursor route has been used to synthesize a series of nanocrystalline rare-earth borates. Amorphous precursor powders are precipitated during an aqueous reaction between RE^{3+} and $NaBH_4$, and the isolated powders can be annealed in air at 700 °C to form YBO_3, $NdBO_3$, $SmBO_3$, $EuBO_3$, $GdBO_3$, and $HoBO_3$. YBO_3:Eu formed using this strategy shows red-orange emission properties that are similar to high-quality nanocrystals prepared by other methods. The materials have been characterized by FTIR spectroscopy, powder XRD, SEM, DSC, UV–Vis fluorimetry, and TEM with EDS and element mapping.

1. Introduction

Due to their crystallographic noncentrosymmetry, metal borates can exhibit nonlinear optical (NLO) properties [1]. While bulk-scale single crystals of NLO materials are most commonly used in optics, polycrystalline NLO materials are gaining increased attention as candidates for use in applications due to an increased efficiency for optical frequency conversion caused by constructive interference [2]. A technological limitation of polycrystalline materials is the ability to maintain the narrow range of wavelengths emitted, which can be influenced by crystal defects and crystal field symmetry [3–5]. Nano- and microcrystalline rare-earth borates have been made by a variety of synthetic methods, including solvothermal reactions [3,6–9], spray pyrolosis [10], single-source precursor decomposition [4,11], and sol–gel synthesis [12]. By decreasing their size to the nanoscale regime, rare-earth borates could have applications as biological fluorescence labels and could provide higher resolution as phosphor components in plasma display panels [9]. However, as a consequence of their size, low crystallinity and surface defects can decrease the luminescence intensity. Therefore, an ideal size range exists where nanocrystalline rare-earth borates can retain optimal luminescence properties, which varies depending on reaction conditions.

Here we describe an alternative method for synthesizing $REBO_3$ (RE = Y, Nd, Sm, Eu, Gd, Ho) by forming an amorphous gel-like precipitate in an aqueous solution of RE^{3+} following the addition of aqueous $NaBH_4$ in the presence of a stabilizing polymer. The dried precipitate is then annealed at 700 °C in air to form $REBO_3$. In addition to the $REBO_3$ phases, we are able to form a nanostructured YBO_3:Eu, a technologically relevant red phosphor [3,4,9,12], that has comparable emission properties to high-quality nanocrystals prepared by solvothermal methods [9]. This simple and general method could be useful for forming application-directed nanostructured materials, such as thin films and patterned surfaces, via deposition and post-annealing of the dispersed nanoscopic precursors.

2. Experimental

Typically, 25–30 mg of rare-earth nitrates or acetates (purities >99.9%, used as received from Alfa Aesar, see Table 1 for details) was dissolved in 30 mL of NANOpure water (reverse osmosis, 18.2 MΩ) with 100 mg poly(vinylpyrrolidone) (40,000 MW, PVP, Aldrich) in an Erlenmeyer flask. After stirring vigorously in air for 15 min, a chilled 10 mL solution of aqueous 0.03–0.09 M $NaBH_4$ (98%, Alfa Aesar) was added dropwise, causing bubbling and often the immediate generation of a translucent precipitate. After stirring for 30–60 min, a translucent gel-like precipitate was isolated via centrifugation at 13 k rpm. The precipitate was not washed so that residual BH_4^- would remain incorporated into the recovered precipitate. After drying in air at 50 °C, the powders

* Corresponding author at: Department of Chemistry, The Pennsylvania State University, University Park, PA 16802, USA. Fax: +1 814 863 8403.
E-mail address: schaak@chem.psu.edu (R.E. Schaak).

0022-4596/$ - see front matter © 2008 Elsevier Inc. All rights reserved.
doi:10.1016/j.jssc.2008.08.028

Table 1
Synthetic details for the formation of amorphous *RE*–B–O powders and thermal transformation to $REBO_3$

RE^{3+} precursor(s)	Mass of $NaBH_4$ (mg) in 10 mL H_2O	Heat treatment	Product
25.5 mg $Y(ac)_3 \cdot 4H_2O$[a]	10.5	700 °C, 90 min	Orthoborate YBO_3
22.8 mg $Eu(NO_3)_3 \cdot 6H_2O$	13.9	700 °C, 90 min	Orthoborate $EuBO_3$
35.2 mg $Nd(NO_3)_3 \cdot 6H_2O$	32.0	700 °C, 2 h	Hexagonal $NdBO_3$
35.4 mg $Sm(NO_3)_3 \cdot 6H_2O$	21.4	700 °C, 2 h	Orthoborate $SmBO_3$
26.2 mg $Gd(ac)_3 \cdot xH_2O$	32.6	700 °C, 90 min	Orthoborate $GdBO_3$
35.3 mg $Ho(NO_3)_3 \cdot 5H_2O$	30.9	700 °C, 90 min	Orthoborate $HoBO_3$
2.2 mg $Eu(NO_3)_3 \cdot 6H_2O$+15.8 mg $Y(ac)_3 \cdot 4H_2O$ (or 11.7 mg $YCl_3 \cdot xH_2O$)	14.0	700 °C, 2 h	Orthoborate YBO_3:Eu

[a] ac = acetate.

were opaque, dense and white except for Ho and Nd, which were pink and purple, respectively. The as-prepared dried powders were then annealed in air at 700 °C for 90–120 min to form $REBO_3$. Specific details for each metal borate system are listed in Table 1.

Powder X-ray diffraction (XRD) data were collected using a Bruker GADDS three-circle X-ray diffractometer (Cu$K\alpha$ radiation) using microdiffraction powder techniques [13]. Transmission electron microscopy (TEM) images and energy-dispersive X-ray spectroscopic (EDS) analysis were collected on a JEOL 2010 TEM operating at 200 kV. Samples were prepared by re-suspending the isolated nanoparticles in ethanol and dropping the solution onto a carbon-coated Ni grid. Scanning electron microscopy (SEM) was performed using an Electroscan ESEM-E3 scanning electron microscope operating at 15 kV. Metal borate powders were prepared for SEM by coating with AuPd using a metal sputter coater. Differential scanning calorimetry (DSC) and thermal gravimetric analysis (TGA) data were collected on a TA Instruments Q600 SDT under flowing air at a heating rate of 10 °C/min. UV absorbance and emission spectra were collected using a Photon Technology International (PTI) fluorimeter with an arc lamp at a scan rate of 1 nm/s. ATR-FTIR spectroscopy was performed using a Bruker TENSOR 27 ATR from 600 to 4000 cm^{-1}.

3. Results and discussion

When aqueous sodium borohydride is added to a solution of Eu^{3+} and PVP in water, the solution changes from clear and colorless to murky, and a translucent gel-like precipitate forms. Under dry reaction conditions, spectroscopic evidence suggests the formation of tetrahydroborate polymeric solid-state structures for some lanthanides in which BH_4^- bridges two metal atoms [14]. The stability of these networks is influenced by how easily the metal cation can be reduced by BH_4^- [14]. In the case of the rare earths, which have a more negative reduction potential than BH_4^- [14], the tetrahydroborate complexes are stable and unreactive. Based on the byproducts from the reaction of BH_4^- with water [15] and the known interactions of RE^{3+} ions with BH_4^- [14], we hypothesize that a polymeric network is forming in solution. One possibility is that byproducts from the reaction of BH_4^- with water bridge RE^{3+} cations to form polymeric networks that precipitate out of aqueous solution as a gel-like solid. ATR-FTIR spectroscopy was used to confirm the presence of B–O groups in the as-prepared samples. Stretches in the region of 1200–1500 cm^{-1} can correspond to both B–O and bridging B–H moieties in the as-prepared powder (Fig. 1, top) [14,16], although additional studies with deuterated sodium borohydride suggest that the moieties present contain oxygen. When annealed to form $EuBO_3$, the stretches in this region decrease in intensity and a new group of signals appears in the 800–1000 cm^{-1} region corresponding to B–O stretches in vaterite-type $EuBO_3$ (Fig. 1, bottom) [17].

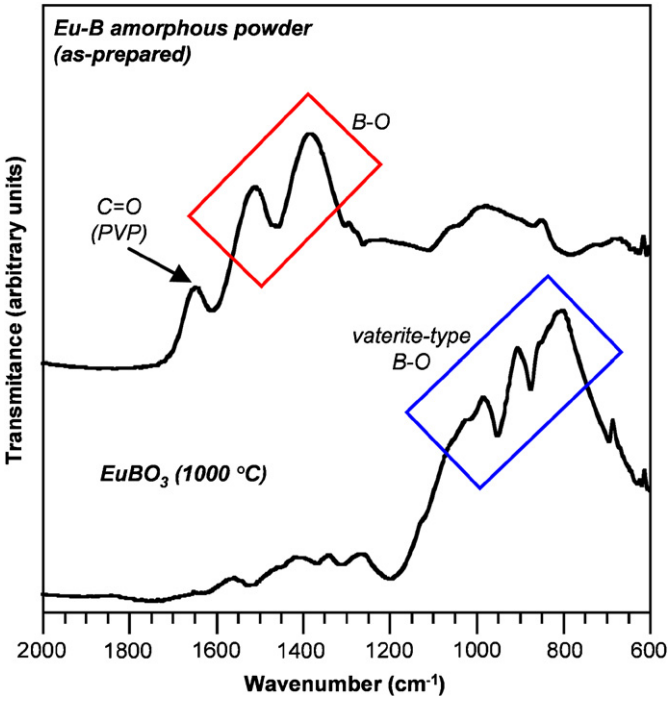

Fig. 1. ATR-FTIR spectra for (top) the as-prepared powder using aqueous $Eu(NO_3)_3$ and $NaBH_4$ and (bottom) $EuBO_3$ after annealing the as-prepared powder at 1000 °C in air to ensure burn-off of PVP. Red and blue boxes indicate regions where B–O stretches and vaterite-type B–O stretches are observed, respectively.

After isolating the gel via centrifugation and dehydrating at 50 °C, the as-prepared powder can be transformed into $EuBO_3$ by thermal treatment in air. As seen in Fig. 2a, the as-prepared powder (top) is amorphous by powder XRD. Heating it to 500 °C begins to crystallize Eu_2O_3, which is further transformed to vaterite-type $EuBO_3$ when heated at 700 °C for 90 min. Typically, using solid-state methods, vaterite-type $EuBO_3$ is reported to form at temperatures above 750 °C [17]. DSC measurements in air show an exotherm at 610 °C (Fig. 2b), corresponding to the crystallization of $EuBO_3$. This transition at 610 °C is at a slightly lower temperature than the exotherm reported for the crystallization of vaterite-type $EuBO_3$ using solid-state synthetic techniques, which occurs near 650 °C [17]. Fig. 3a shows a TEM image of the as-prepared amorphous Eu–B–O powder, which is made up of a web-like network of smaller particles. An SEM image (Fig. 3b) of vaterite-type $EuBO_3$ formed by heating at 700 °C shows that the product roughly retains the network-like morphology of its precursor.

In addition to $EuBO_3$, other rare-earth borates can be formed using this method. YBO_3, $GdBO_3$, $HoBO_3$, $SmBO_3$ and $NdBO_3$ can be made by annealing their respective amorphous powder precursors

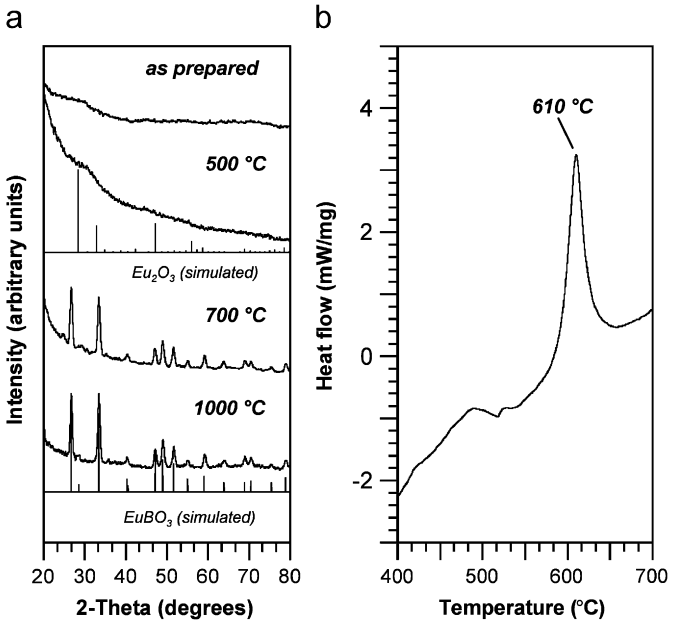

Fig. 2. (a) Powder XRD patterns characterizing the synthesis of $EuBO_3$ from an amorphous Eu–B–O powder. The as-prepared powder (top) was annealed at 500, 700 and 1000 °C in air. Crystalline $EuBO_3$ was formed at 700 °C. (b) DSC trace for the as-prepared powder collected under flowing air showing an exotherm at 610 °C, correlating to the crystallization of orthoborate $EuBO_3$.

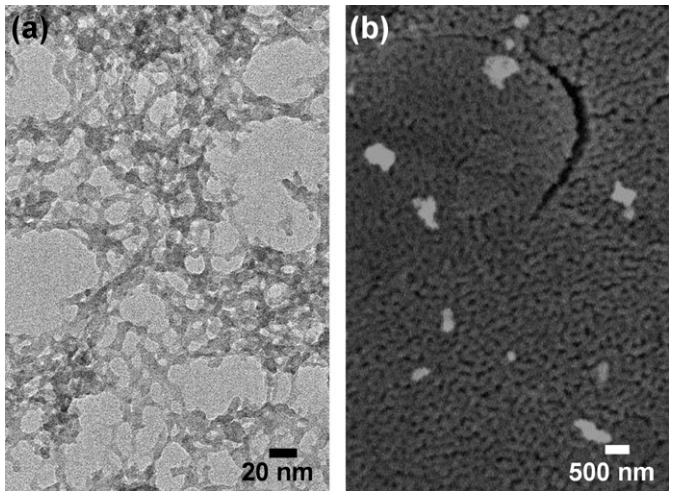

Fig. 3. (a) TEM image of the as-prepared Eu–B–O powder. (b) SEM image of porous $EuBO_3$ prepared by annealing the powder from (a) at 700 °C in air for 90 min.

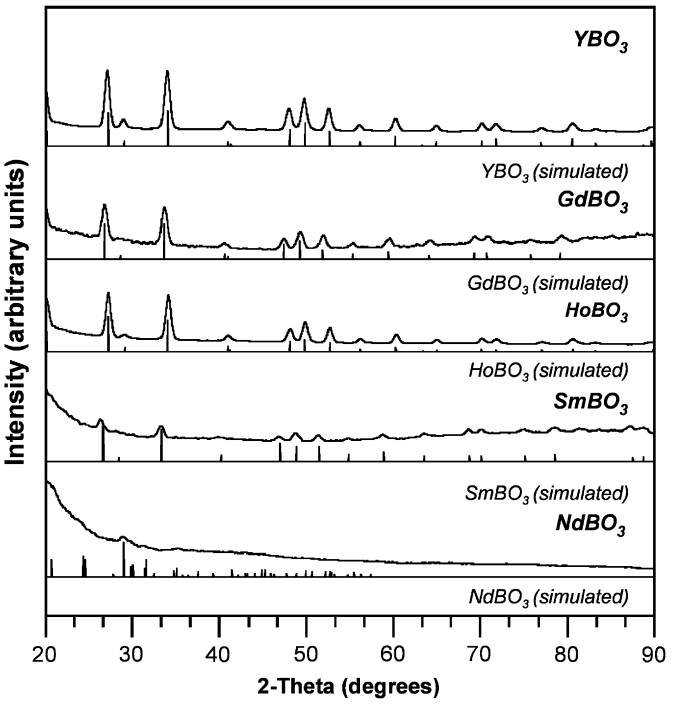

Fig. 4. Powder XRD patterns for other *RE*BO_3 phases accessible by annealing amorphous precursor powders at 700 °C in air for 90–120 min. Simulated XRD patterns are shown below experimental data.

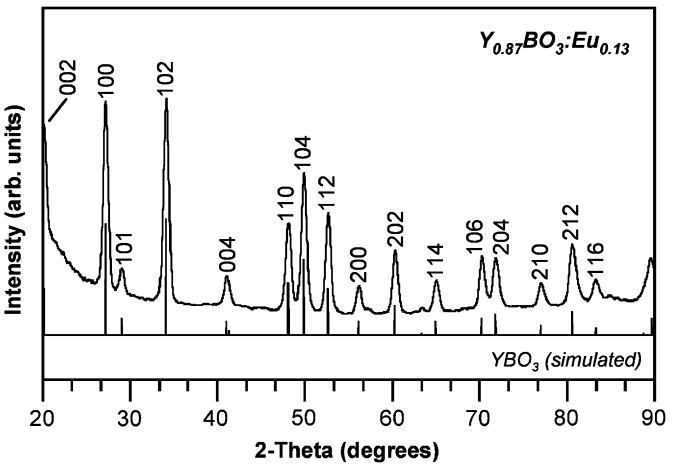

Fig. 5. Powder XRD pattern for Eu-doped YBO_3 after annealing at 700 °C for 2 h in air. The simulated XRD pattern for YBO_3, PDF card no. 16-277, is shown for comparison.

at 700 °C (Fig. 4). All crystallize as orthoborate phases, except $NdBO_3$, which preferentially forms a hexagonal phase that does not have NLO properties. All products are white, except Ho–B–O and Nd–B–O, which retain the color of their $Ho(NO_3)_3$ and $Nd(NO_3)_3$ precursors, respectively. This is credited to 4*f* transitions in the Ho^{3+} and Nd^{3+} ions [15]. However, the color disappears when the amorphous powders are annealed to form $HoBO_3$ and $NdBO_3$, which are both white solids.

The *RE*BO_3 orthoborates are noncentrosymmetric, which can result in NLO properties [1]. Of particular technological interest are orthoborates doped with rare-earth cations because they can be used as phosphors. When irradiated with UV light, YBO_3:Eu emits in the red-orange region of the visible spectrum [3,4,9,12]. A promising red phosphor for use in plasma display panels, YBO_3:Eu has a strong luminescent intensity, a high optical damage threshold, vacuum-UV transparency, and chemical stability [9]. The quality of emission from YBO_3:Eu is related to its crystallinity and the symmetry around the Eu^{3+} cations [3,4]. The strongest UV-emission bands in the visible range observed for YBO_3:Eu are at 592, 612 and 624 nm. The orange emission at 592 nm corresponds to a magnetic dipole transition, whereas the red emission at 612 nm corresponds to an electric dipole transition [3]. Local crystal field symmetry around the Eu^{3+} cations can have a significant effect on electric dipole transitions [3]. For example, bulk-scale single crystals have high local symmetry around the Eu^{3+} cations, which diminishes the intensity of the red emission. However, when the crystal size is decreased to nanoscale dimensions, surface defects decrease the local symmetry around the Eu^{3+} cations, increasing the intensity of the red emission [3,9]. For use in plasma displays, it

is important that the YBO_3:Eu have a strong red emission component [4].

Using our synthetic protocol, we were able to synthesize YBO_3 doped with Eu^{3+} by annealing the as-prepared powder at 700 °C in air for 2 h (Fig. 5). This results in the precipitation of networks of small particles (~10–20 nm in diameter), as seen in Fig. 6a. The homogeneous incorporation of Y and Eu is confirmed by EDS mapping, showing an 87:13 Y:Eu ratio (Fig. 6b–d). When annealed, the resulting powder retains the periodic voids defined by the nanoparticle networks and is composed of constituent particles that are ~500 nm in diameter (Fig. 7). A UV-emission spectrum (Fig. 8) obtained by irradiating YBO_3:Eu particles

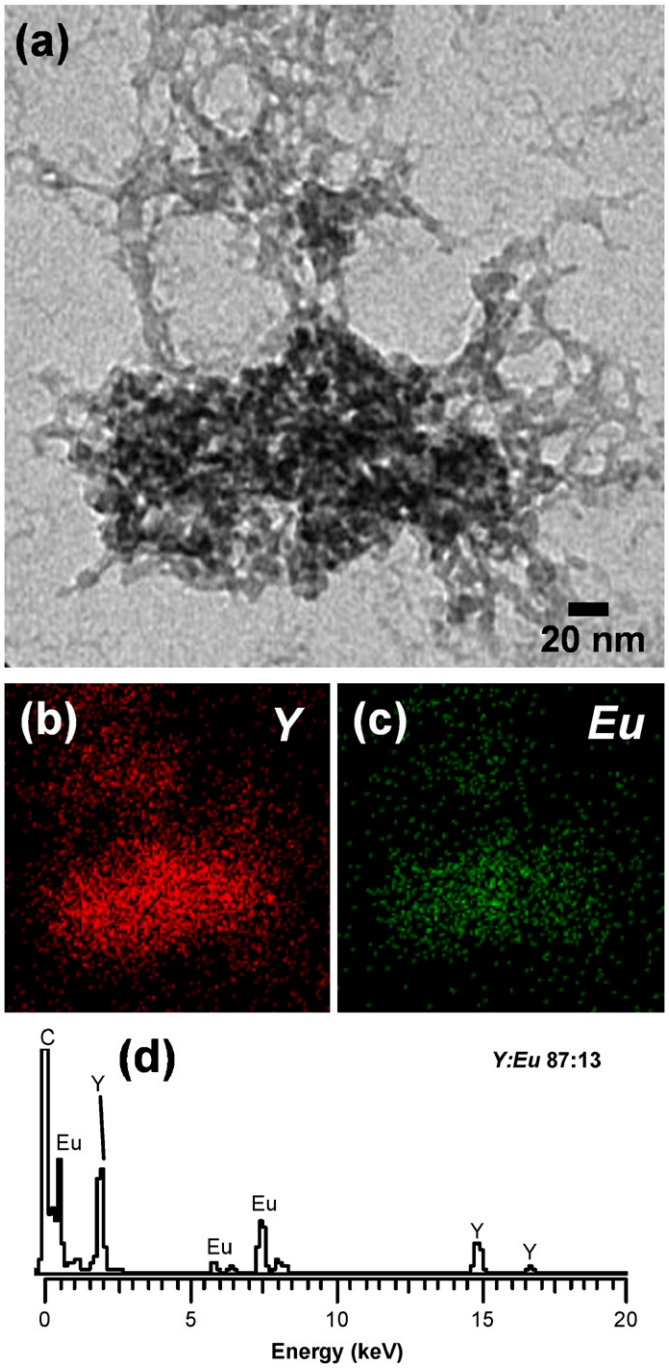

Fig. 6. (a) TEM image of as-prepared Y–Eu–B–O powder with EDS maps showing the presence of both (b) Y and (c) Eu homogeneously distributed in the sample; (d) EDS spectrum showing a Y:Eu ratio of 87:13.

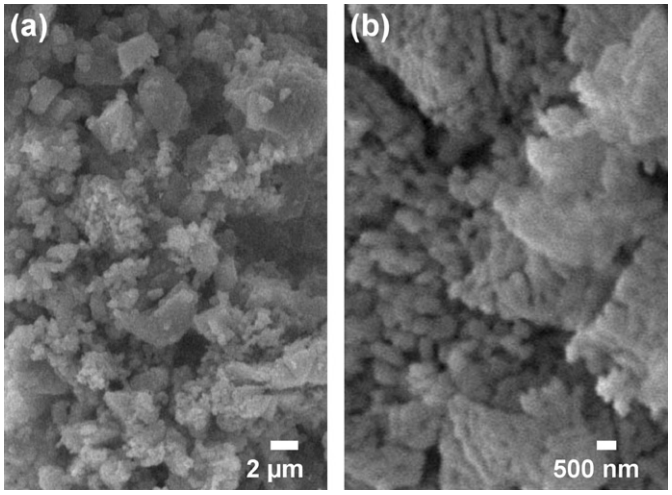

Fig. 7. SEM images of nanocrystalline YBO_3:Eu powder taken at (a) 2.8k and (b) 9k magnification.

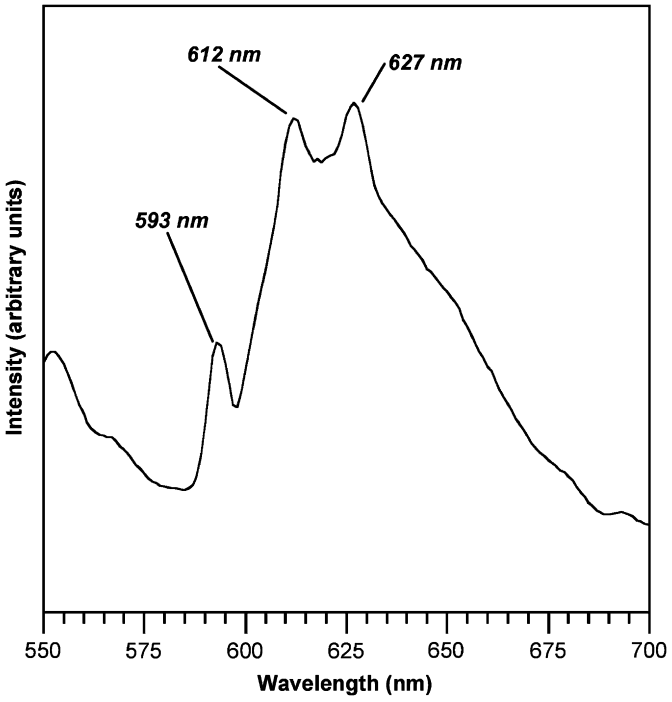

Fig. 8. Emission spectrum for YBO_3:Eu (dispersed in isopropanol) collected under 254-nm UV irradiation. Peaks at 593 and 612 nm correlate to orange and red emissions, respectively.

dispersed in isopropanol with 254-nm light shows emission bands at 593, 612 and 627 nm, which correlate well with previous literature reports [9]. The dominant red emission at 612 nm is in accordance with recent reports of emission spectra for 8 nm YBO_3:Eu nanocrystals prepared by solvothermal methods [9].

4. Conclusions

Here we have described a simple aqueous precursor strategy that was developed for synthesizing amorphous rare-earth borate powders, which can be annealed to form *RE*BO_3 powders that retain the network-like structure of their precursors. It is hypothesized that the amorphous precursor is made up of a

polymeric network of RE^{3+} and B–O species formed from the reaction of BH_4^- with RE^{3+} cations in water, which facilitates conversion into the $REBO_3$ products. Due to their NLO properties, rare-earth orthoborates can be used as red phosphors in plasma displays. Of particular importance is the formation of YBO_3:Eu using this strategy, which has a red-orange emission comparable to literature reports [9]. Preliminary evidence suggests that other metals can be introduced into the amorphous *RE*–B powder, resulting in a multi-metal precursor that can be used to form huntite-type $Al_3RE(BO_3)_4$. The simplicity of this strategy for synthesizing $REBO_3$ and the nanocrystalline particle sizes could also make it useful for forming thin films and patterned substrates.

Acknowledgments

This work was supported by a NSF CAREER Award (DMR-0545201 and DMR-0728943) and the Robert A. Welch Foundation (Grant no. A-1583). This material is based upon work supported under a NSF Graduate Fellowship to A.E.H. Partial support was also provided by the Arnold and Mabel Beckman Foundation (Young Investigator Award) and DuPont (Young Professor Grant). Electron microscopy was performed at the Texas A&M Microscopy and Imaging Center. UV-emission spectroscopy was performed at the TAMU/CIMS Materials Characterization Facility. The authors thank Dr. Rick Littleton at the Microscopy and Imaging Center for assistance with collecting SEM data, Dr. Gang Liang at the TAMU/CIMS Materials Characterization Facility for assistance with collecting UV-emission data, and Casey Wade for assistance with collecting ATR-FTIR data.

References

[1] P. Becker, Adv. Mater. 10 (1998) 979–992.
[2] M. Baudrier-Raybaut, R. Haïdar, P. Kupecek, P. Lemasson, E. Rosencher, Nature 432 (2004) 374–376.
[3] X.-C. Jiang, C.-H. Yan, L.-D. Sun, Z.-G. Wei, C.-S. Liao, J. Solid State Chem. 175 (2003) 245–251.
[4] Z. Wei, L. Sun, C. Liao, C. Yan, S. Huang, Appl. Phys. Lett. 80 (2002) 1447–1449.
[5] G. Chadeyron, R. Mahiou, M. El-Ghozzi, A. Arbus, D. Zambon, J.C. Cousseins, J. Lumin. 72 (1997) 564–566.
[6] T. Kim, S. Kang, Mater. Res. Bull. 40 (2005) 1945–1954.
[7] X.-C. Jiang, L.-D. Sun, C.-H. Yan, J. Phys. Chem. B 108 (2004) 3387–3390.
[8] F. Wang, X. Fan, D. Pi, M. Wang, J. Solid State Chem. 177 (2004) 3346–3350.
[9] Z. Li, J. Zeng, Y. Li, Small 3 (2007) 438–443.
[10] (a) D.S. Kim, R.Y. Lee, J. Mater. Sci. 35 (2000) 4777–4782;
(b) K.N. Kim, H.K. Jung, H.D. Park, D. Kim, J. Mater. Res. 17 (2002) 907–910.
[11] Z.G. Wei, L.D. Sun, C.H. Liao, X.C. Jiang, C.H. Yan, J. Mater. Chem. 12 (2002) 3665–3670.
[12] D. Boyer, G. Bertrand, R. Mahiou, J. Lumin. 104 (2003) 229–237.
[13] (a) N.S.P. Bhuvanesh, J.H. Reibenspies, J. Appl. Crystallogr. 36 (2003) 1480–1481;
(b) N.S.P. Bhuvanesh, J.H. Reibenspies, Y. Zhang, P.L. Lee, J. Appl. Crystallogr. 38 (2005) 632–638.
[14] T.J. Marks, J.R. Kolb, Chem. Rev. 77 (1977) 263–293.
[15] F.A. Cotton, G. Wilkinson, Advanced Inorganic Chemistry, Wiley, New York, 1988.
[16] N.M.D. Brown, P. Bladon, J. Chem. Soc. (A) (1969) 526–532.
[17] S. Lemanceau, G. Bertrand-Chadeyron, R. Mahiou, M. El-Ghozzi, J.C. Cousseins, P. Conflant, R.N. Vannier, J. Solid State Chem. 148 (1999) 229–235.